Research Article

Ridwan Ridwan, Aditya Rio Prabowo*, Nurul Muhayat, Teguh Putranto, and Jung Min Sohn

Tensile analysis and assessment of carbon and alloy steels using FE approach as an idealization of material fractures under collision and grounding

https://doi.org/10.1515/cls-2020-0016
Received Aug 15, 2020; accepted Oct 14, 2020

Abstract: In this study, a numerical investigation tensile test using ANSYS on three different carbon and alloy sheets of steel: AISI 1030 medium carbon steel, AISI 1080 high carbon steel and high-strength low-alloy (HSLA) A606 steel, has been carried out. The influences of three different specimen geometries on the stress–strain curve were also investigated. Understanding the properties of these materials, such as stress–strain obtained from a tensile test, is important. Materials are subjected to forces or loads when in use, for example, steel in a ship's hull experiences significant stresses and strains. In such situations, it is necessary to understand the characteristics of the material because grounding or collisions can occur, which deform the materials. The differences in stress and strain obtained from three specimens with different geometries and mesh sizes of 2.5, 5, 7.5, and 10 mm for all proposed steels, were observed. The results showed that the ultimate tensile strength was always lower in specimen 2 compared to the other specimens. Furthermore, the highest von Mises stress and strain contour was located in the midsection of specimens 1 and 3 in all of the proposed materials.

Keywords: tensile test, carbon steel, finite element method, stress-strain

1 Introduction

Researchers and vehicle designers have gone to great efforts to explore the safety characteristics of several motor vehicles [1]. Often, two groups of methods are used to quantify the impacts of these characteristics on vehicle safety [2]. The first is based on testing the ability of a vehicle to avoid a crash at the pre-crash stage (crash avoidance) and the second is to protect its occupants at the post-crash stage (crashworthiness). In crashworthiness, the material used in the vehicle design can be damaged when a crash or collision occurs. The maritime transportation system is a critical component of transport worldwide and has an important contribution to the global economy which is covering more than 90% of international trade [3]. Approximately 11 billion tons of cargo was transported by sea in 2018 [4]. The efficiency and capacity of maritime transportation continues to develop with the growth of global trade activities and new technologies. Furthermore, shipping is one of the most important modes of transportation,.Over recent years, studies on maritime transportation, especially covering ship accidents, have been carried out [5–9]. However, the maritime transportation system (MTS) poses several risks as it consists of several elements related to humans, ships, the environment, and management. As a consequence, this system is vulnerable to several types of hazard, many of which can result in accidents such as collisions, groundings, contacts, sinking, and fires [10]. Moreover, maritime accidents create unavoidable risks for individuals and society in terms human and economic losses, and negative environmental consequences [11].

***Corresponding Author: Aditya Rio Prabowo:** Department of Mechanical Engineering, Universitas Sebelas Maret, Surakarta 57126, Indonesia; Email: aditya@ft.uns.ac.id
Ridwan Ridwan: Graduate School of Mechanical Engineering, Universitas Sebelas Maret, Surakarta 57126, Indonesia
Nurul Muhayat: Department of Mechanical Engineering, Universitas Sebelas Maret, Surakarta 57126, Indonesia
Teguh Putranto: Department of Civil Engineering and Architecture, Tallinn University of Technology, Tallinn 19086, Estonia; Department of Naval Architecture, Institut Teknologi Sepuluh Nopember, Surabaya 60111, Indonesia
Jung Min Sohn: Department of Naval Architecture and Marine Systems Engineering, Pukyong National University, Busan 48513, South Korea

Recent computation power improvements have made it practical to carry out finite element modeling of large marine structures subjected to a collision. Since experimental tests in actual-scale marine structures demand heavy financial investment, heavy-duty equipment, and complicated logistics [12], reduced scale applications are particularly important in marine engineering. Experimental studies of the crashworthiness of marine structures most often deal with collision tests in simplified structures, and their aim is to represent sections of an actual marine structure. Tensile strength testing is one of the most important engineering tests used for metallic materials to obtain the material's characteristics. During a tensile test, a specimen is subjected to a controlled tension until failure, providing material characteristics such as yield strength, ultimate tensile strength, and strain at break.

In this paper, we assess the performance of three steel materials (*i.e.*, AISI 1030 medium carbon steel, AISI 1080 high carbon steel and high-strength low-alloy (HSLA) A606) in tensile tests using a numerical approach with ANSYS software. The different geometries of the specimen are also considered in the numerical approach. The influence of the mesh size on the values of the stress–strain curve in the steel materials are analyzed and we then summarize the results.

(a)

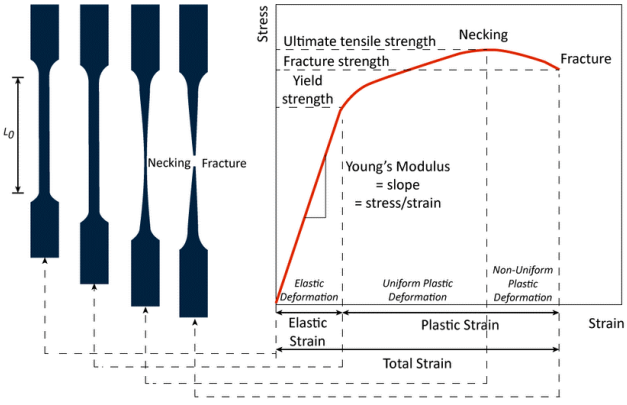

(b)

Figure 1: (a) The uniaxial tensile test sample and tensile testing machine [13], and (b) the shape of the specimen changes during tensile testing [14]

2 Literature review

2.1 Tensile test

Materials are subjected to forces or loads when in service, for example, steel in a ship hull experiences significant stresses. In such situations, it is necessary to know the stress–strain characteristics of the material because grounding, impact, or collision can occur, deforming the materials. One of the most common mechanical stress–strain tests is performed using tension. The tension test can be used to ascertain several mechanical properties of materials that are important in design. In the tension test, a specimen is deformed with a tensile load that is applied uniaxially along the long axis of a specimen, usually until a fracture occurs. The output of a tensile test is recorded as a load or force versus elongation. The load and elongation are normalized to the respective parameters of engineering stress and engineering strain. Figure 1a shows the uniaxial tensile test sample and the tensile testing machine that is used to obtain a stress–strain curve. Figure 1b shows the changes in shape of the specimen during tensile testing.

Engineering stress σ is defined by Equation 1.

$$\sigma = \frac{F}{A_0}, \tag{1}$$

where F is the instantaneous load applied perpendicular to the specimen cross-section and A_0 is the original cross-sectional area before any load is applied. Engineering strain ϵ is defined by Equation 2.

$$\epsilon = \frac{l_i - l_0}{l_0} = \frac{\Delta l}{l_0} \tag{2}$$

where l_0 is the original length before any load is applied and Δl is the deformation elongation or change in length at some instant, as referenced to the original length [15].

2.2 Crashworthiness

Crashworthiness is the degree to which a transportation model or vehicle will protect its occupants from the effects of an accident. While in the ship, crashworthiness can be described as the ability of the structure to protect its cargo,

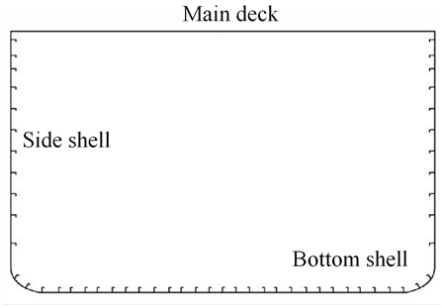

(a)

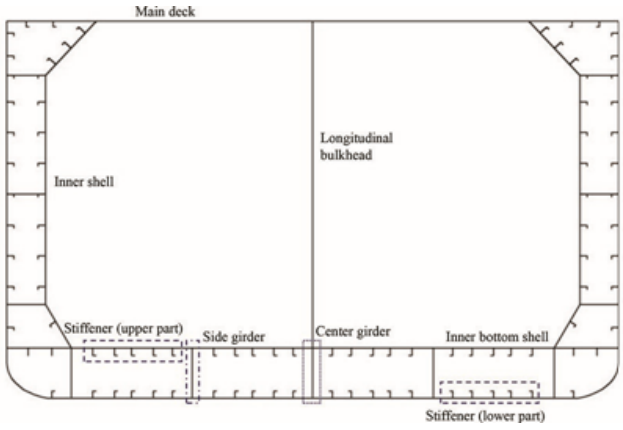

(b)

Figure 2: Illustrations of (a) a single-hull design [21] and (b) the midship section of a double hull tanker [22]

passengers, crew, or other important entities during an accident. There is great demand (both private and public) to reduce the risk of loss of human life and oil spillages at sea and to minimize the damage caused by groundings or collisions of the ship. Over the past decade, regulations covering ship designs have been strengthened in the United States (U.S.). One of the regulations—the use of the double hull structure—was enacted by the Oil Pollution Act in 1990, which requires that all new oil tankers operating in U.S. waters be designed with a double hull. Figure 2 shows illustrations of the single hull and double hull ship design. Furthermore, the increased demand for safety of marine transportation, especially in terms of ships and marine pollution, is closely related to environmental issues associated with disasters due to oil spillage. This has led to improvements in crashworthiness both in terms of hull structures and rescue operations. In ship–ship collisions or grounding events, the impact energy is mainly absorbed by large structural deformations in the ships' structure.

An illustration of a ship–ship collision is shown in Figure 3. Over the last few decades, efforts have been made to develop reliable analysis tools and procedures for evaluating the response of hull structures during accidental load-

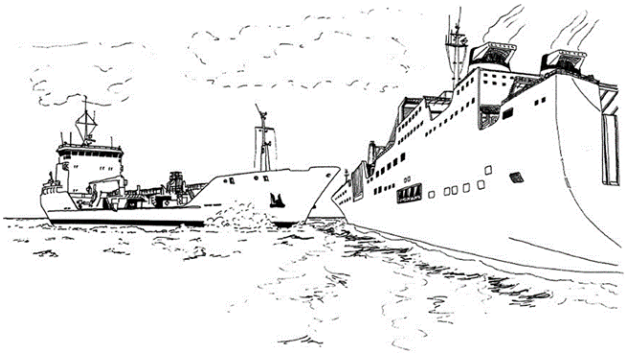

Figure 3: Illustration of a ship–ship collision [23]

ing [16]. Nevertheless, understanding the stress–strain of a material in which tensile load is applied uniaxially along the long axis of a specimen until a fracture occurs is still an important characteristic. Furthermore, various methods have been developed to analyze the structure of ship crashworthiness and internal mechanics during grounding and collision events.By knowing and controlling the structural behavior of ship hull structures during groundings and collisions, ship safety can be improved. It is very important to conduct research on the risk analysis of accidents and provide decision support for maritime safety management [17–20].

3 Benchmark study

3.1 Experiment and analysis profile

In this work, we validated our numerical simulation using ANSYS by comparing our results with a previous benchmark study by Jose and Anto [24]. The test was conducted by increasing the load to pull the specimen until a fracture occurred. The specimen created for this tensile test is shown in Figure 4 and the dimensions of the specimen are listed in Table 1. The material properties of the specimen in this study are described in Table 2. To obtain a variety of results, mesh sizes of 2.5, 5, 7.5, and 10 mm were chosen to be applied to the numerical models. The results of the nu-

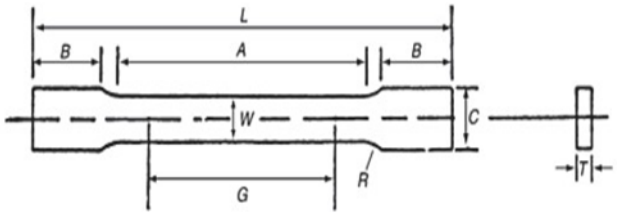

Figure 4: Specimen created for the tensile test [24]

Table 1: Dimensions of the specimen tested [24]

Description	Overall length (L)	Length of reduced section (A)	Length of grip section (B)	Gauge length (G)	Width (W)	Width of grip section (C)	Radius of fillet (R)	Thickness (T)
Dimensions [mm]	457	229	76	203	35	51	25	10

Table 2: Material properties of the specimen tested [24]

Material	Density (kg/m^3)	Young's modulus (GPa)	Poisson's ratio	Yield strength (MPa)	Plastic strain
Mild steel	7860	211	0.28	247	0.02

merical calculation were compared in terms of the value of von Mises stress, stress, and strain. This discussion will be presented in the next section.

3.2 Results

The results of the numerical calculation of the tensile test in the current study and the benchmark test from the previous study by Jose and Anto [24] are summarized and compared in Table 3. The results based on the simulations of the tensile test presented a good correlation with the previous study [24]. As listed in Table 3, the value of von Mises stress, stress, and strain of the specimen in the mesh size 7.5 and 10 mm produced the most similar to the previous study. Further, it was obtained that the mesh size 2.5 and 5 mm produced a higher value of von Mises stress and stress. The overall results suggest that the present methodology in conducting the finite element simulation has successfully produced similarity result with the previous study by Jose and Anto [24]. The configuration and setting of the benchmark will be applied further in the tensile test study.

4 Analysis preparation

4.1 Geometry and material

Specimens with three different geometries were used in this study. The dimensions of the specimens are shown in Figure 5, and those shown in Figure 5a, 5b have both been used before in the numerical analysis of ship collision and

Table 3: Benchmark study's result and the results of the current tensile test

	Mesh size (mm)	Minimum			Maximum		
		von Mises (MPa)	Stress (MPa)	Strain (-)	von Mises (MPa)	Stress (MPa)	Strain (-)
Benchmark data referred to [24]	N/A	N/A	N/A	N/A	205.8	182	1.48
Current FE analysis	2.5	4.5	−21.3	0.0	342.1	353.1	1.5
	5	5.0	−21.1	0.0	339.5	332.0	1.5
	7.5	5.1	−39.5	0.0	199.0	179.0	1.5
	10	1.1	−85.6	0.0	194.8	184.0	1.5

Table 4: Material properties of the proposed carbon and alloy steels

Material	Steel grade	Density (kg/m^3)	Young's modulus (GPa)	Yield strength (MPa)	Ultimate strength (MPa)	Poisson's ratio (-)
Medium carbon steel	1030	7850	206	345	550	0.29
High carbon steel	1080	7850	205	585	965	0.29
High-strength low-alloy	A606	7870	205	310	448	0.28

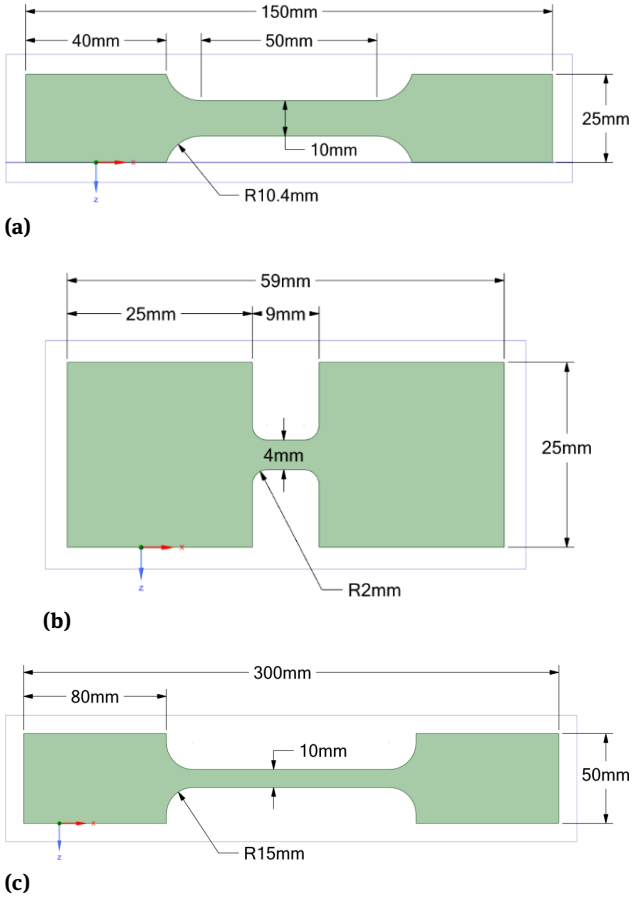

Figure 5: The geometry of specimen tested: (a) Specimen 1; (b) Specimen 2; (c) Specimen 3

grounding [25, 26]. Figure 5c shows a specimen that was used in a study of tensile tests conducted by Iannucci *et al.* [27].

We also used three types of steel in the tests, *i.e.*, medium-carbon, high-carbon, and high-strength low-alloy (HSLA). The properties of these materials are presented in Table 4.

4.2 Scenario and boundary conditions

The tensile test was defined as the opposite axial load acting on both sides of the specimen gauge length until a fracture occurs. The meshing size was determined to be 2.5, 5, 7.5, and 10 mm for the specimens. We measured the stress–strain, von Mises contour and strain contour.

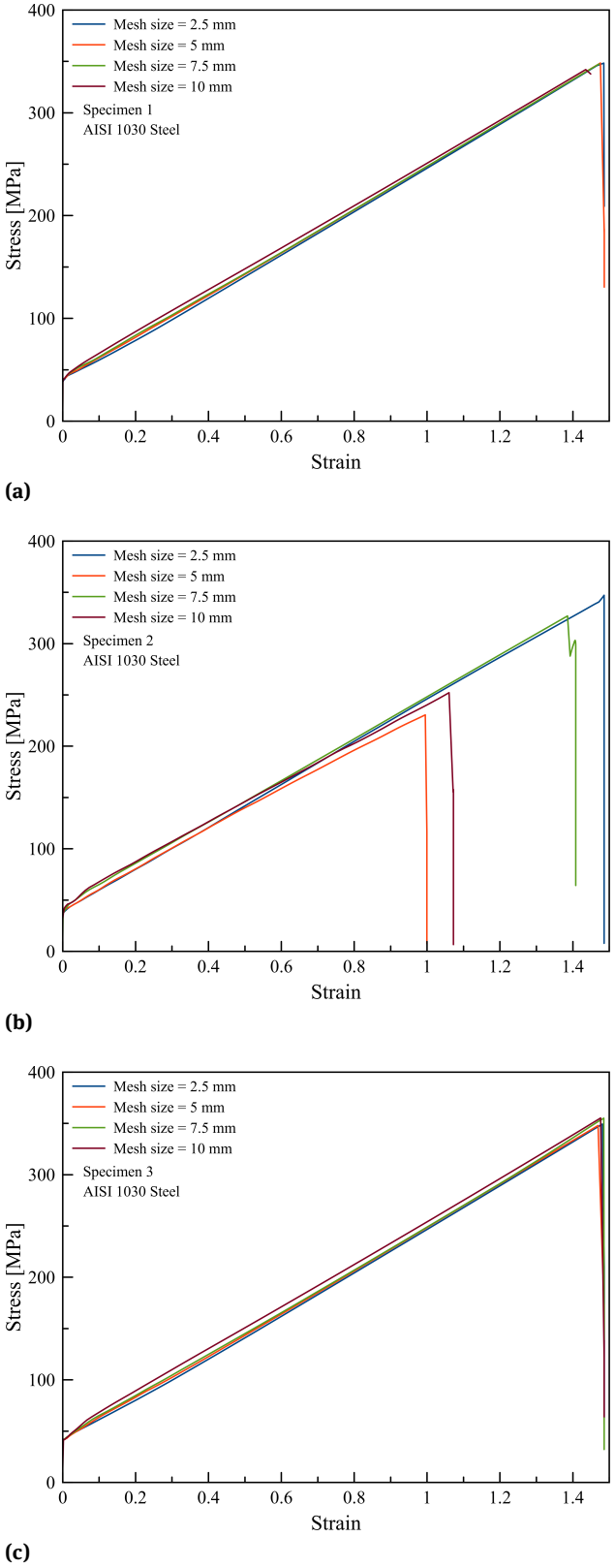

Figure 6: Geometry characteristics of all three specimens with AISI 1030 steel: (a) Specimen 1; (b) Specimen 2; (c) Specimen 3

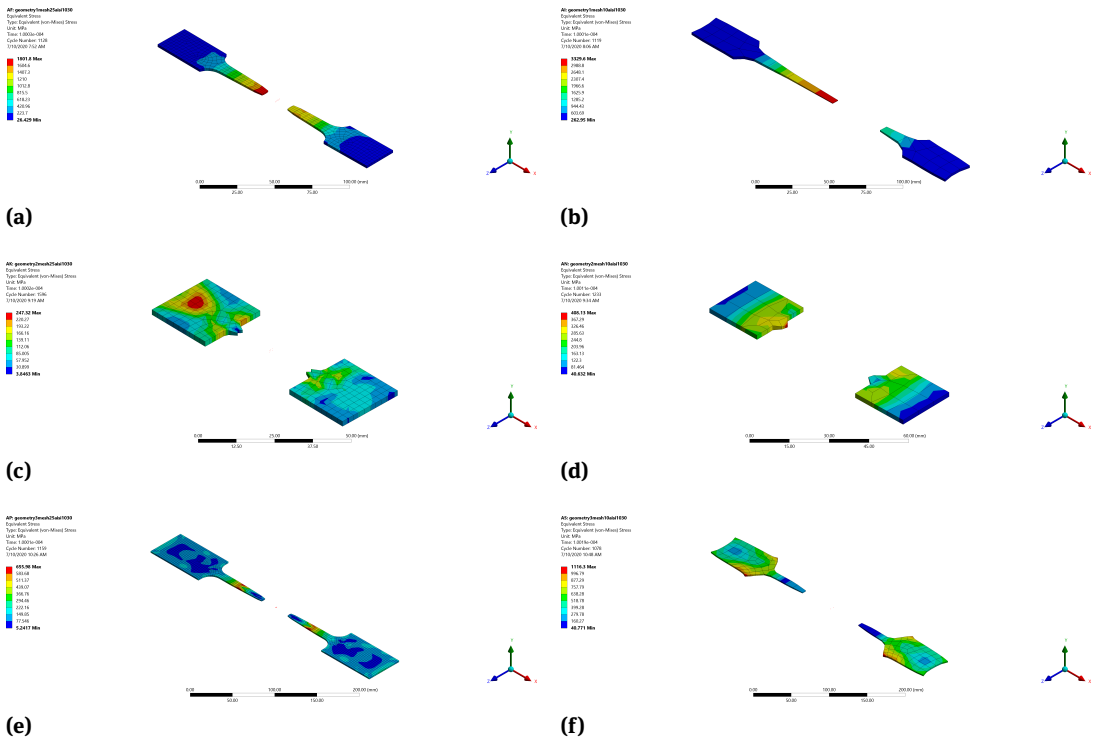

Figure 7: Von Mises contour of the specimens with AISI 1030 steel (mesh size 2.5 and 10 mm): (a-b) Specimen 1; (c-d) Specimen 2; (e-f) Specimen 3

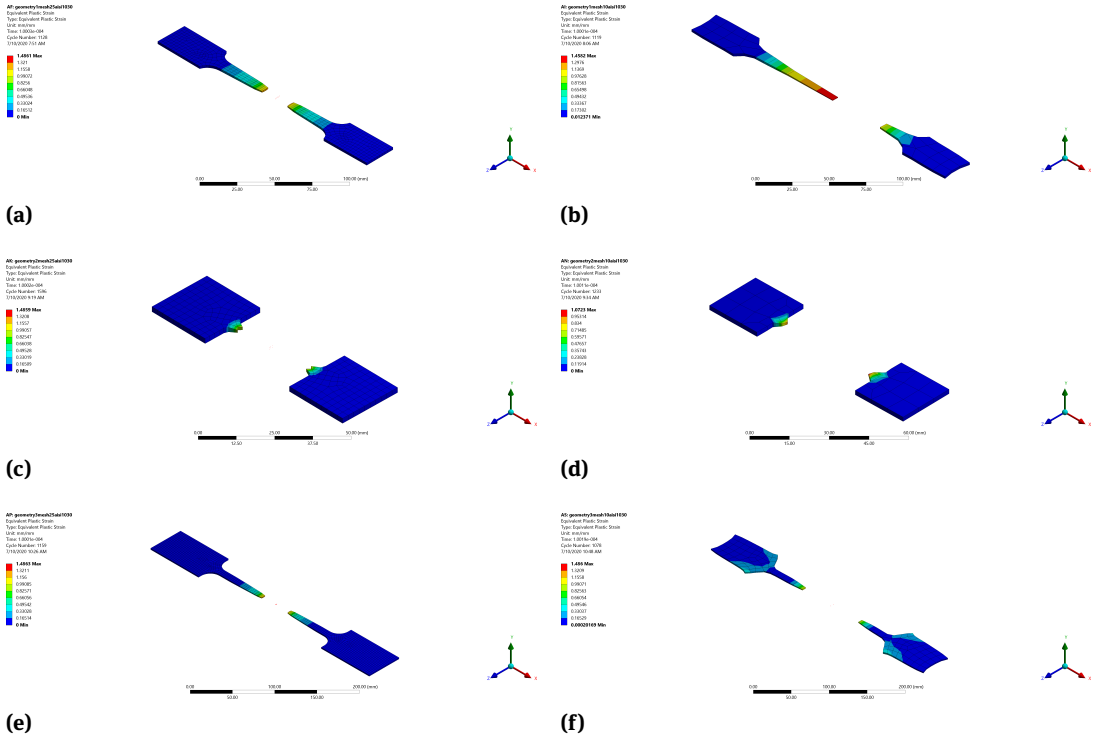

Figure 8: Strain contour of the specimens with AISI 1030 steel (mesh size 2.5 and 10 mm): (a-b) Specimen 1; (c-d) Specimen 2; (e-f) Specimen 3

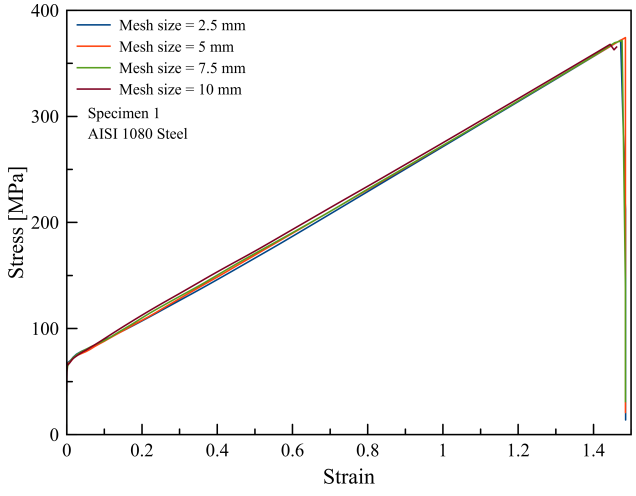

(a)

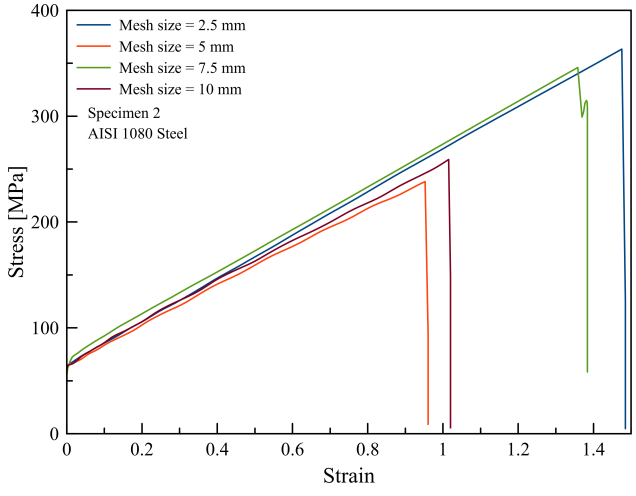

(b)

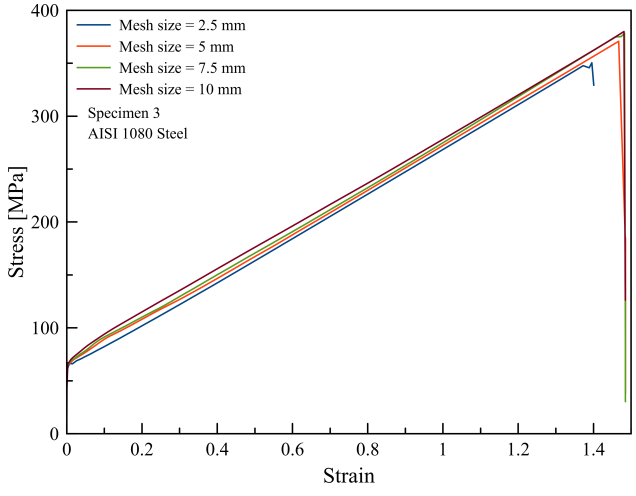

(c)

Figure 9: Geometry characteristics of all three specimens with AISI 1080 steel: (a) Specimen 1; (b) Specimen 2; (c) Specimen 3

5 Results and discussion

5.1 Geometry characteristic

Figure 6a, 6c shows that with the geometry of specimens 1 and 3 and AISI 1030 steel, fractures occurred at a load of 348.3 MPa and strain of 1.48. With the geometry of specimen 2, fractures occurred at a load of 347.13 MPa and strain of 1.49 when the mesh size was 2.5 mm. For the same example, when the mesh size was 5, 7.5, and 10 mm, fractures occurred at 230.5 MPa, 252.2 MPa, and 326.9 MPa, respectively, as shown in Figure 6b. The von Mises stress contours, which represent failure due to stress, are presented in Figure 7. The concentration of von Mises stress contours in specimen 1 were mainly found in the center of the reduced section of the specimen, and stress had started to expand and reached the grip section. A similar pattern was found for specimen 3 and a mesh size of 2.5 mm, in which the highest von Mises stress was located in the midsection. However, for specimen 2, the von Mises stress was found to be widely distributed across almost the entire specimen. An observation of the strain contour also indicated that there was a significant difference in terms of the contour obtained when specimen 2 had a mesh size of 10 mm, as shown in Figure 8. Even so, the biggest strain contour was mainly located in the midsection for all of the specimens.

5.2 Applied material

Figure 9a,c shows that for specimens 1 and 3 with AISI 1080 steel, fractures occurred at a load of around 374.3 MPa and a strain of 1.48. With regard to specimen 2, fractures occurred at a load of around 363.3 MPa and a strain of 1.47 when the mesh size was 2.5 mm. For the same specimen, when the mesh size was 5, 7.5, and 10 mm, fractures occurred at 238.2 MPa, 345.9 MPa, and 259.1 MPa, respectively, as shown in Figure 9b. A similar pattern of von Mises stress contours was found in specimens 1 and 3 with material AISI 1080 and HSLA A606, as presented in Figures 10 and 11, respectively.

It was found that the highest von Mises stress was located in the center of the reduced section of the specimens, and the stress started to expand and reached the grip section. A similar pattern was found for the strain contour, as shown in Figures 12 and 13. The most significant strain contour was mainly located in the midsection of the specimens. However, specimen 2 with a 10 mm mesh size showed a different pattern.

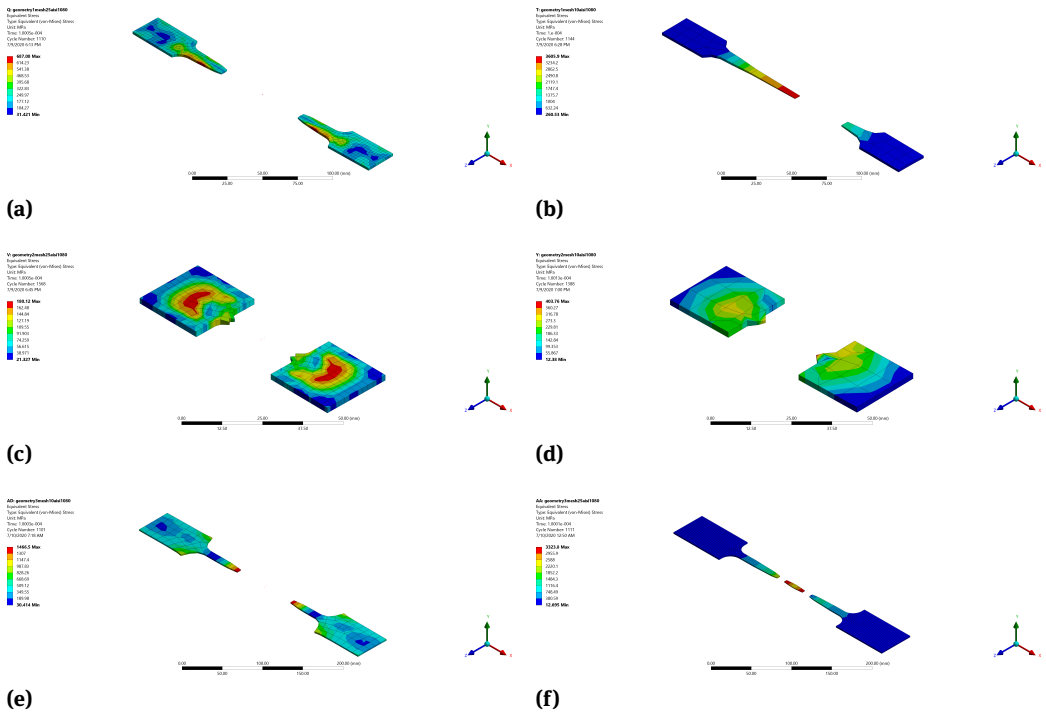

Figure 10: Von Mises contour of the specimens with AISI 1080 steel (mesh size 2.5 and 10 mm): (a-b) Specimen 1; (c-d) Specimen 2; (e-f) Specimen 3

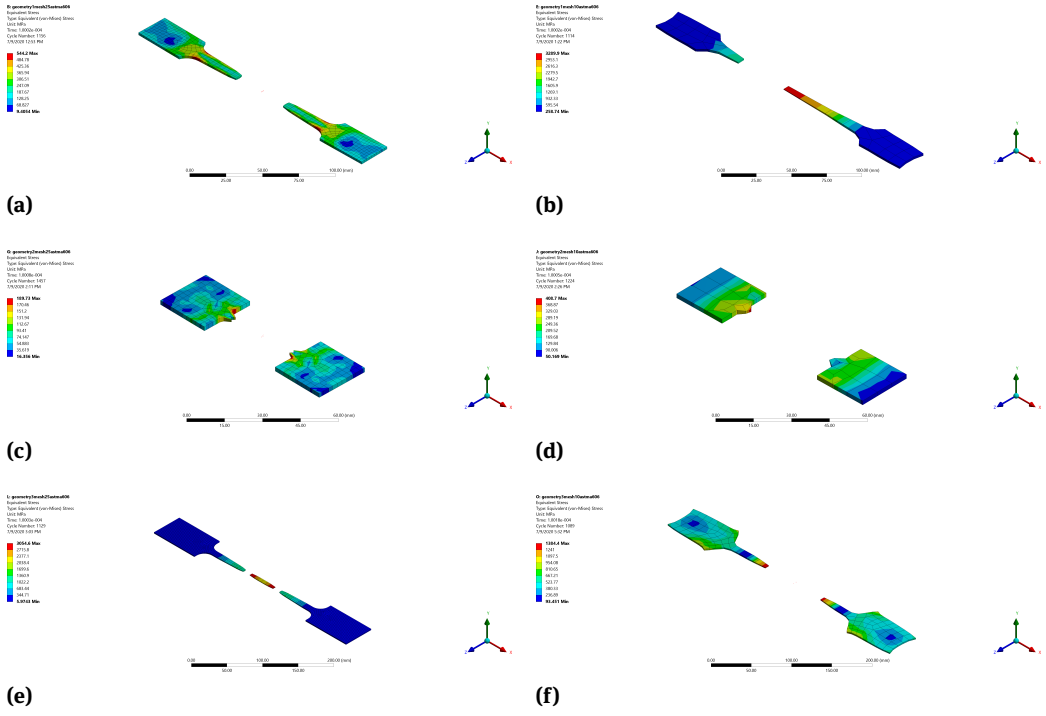

Figure 11: Von Mises contour of the specimens with HSLA A606 steel (mesh size 2.5 and 10 mm): (a-b) Specimen 1; (c-d) Specimen 2; (e-f) Specimen 3

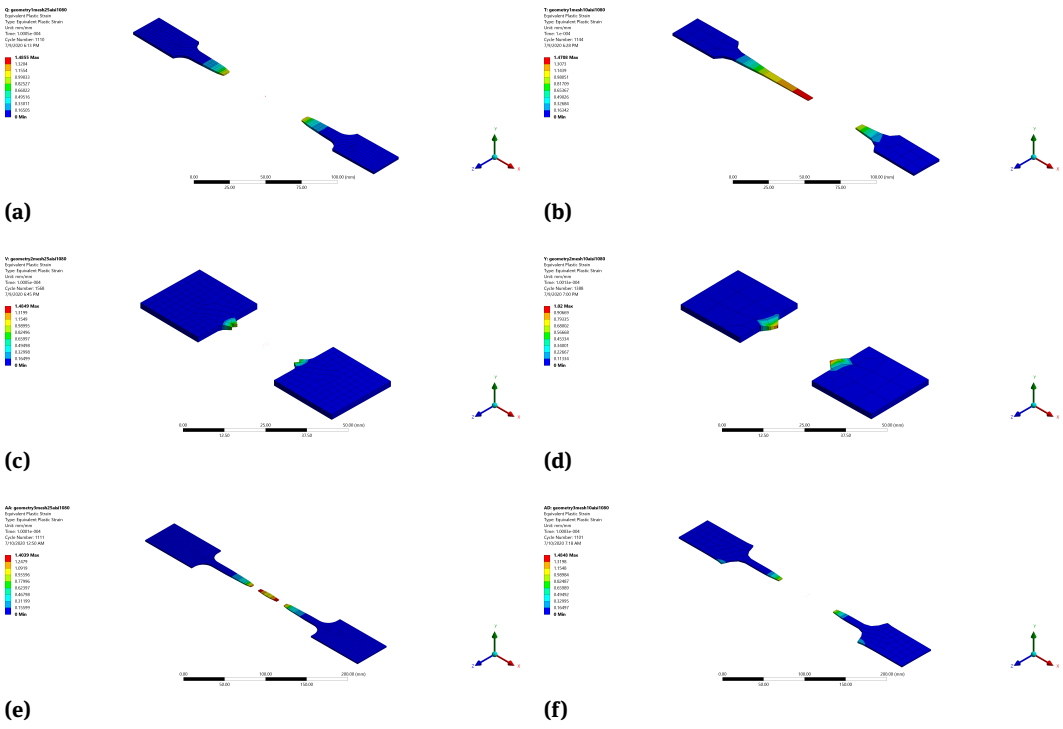

Figure 12: Strain contour of the specimens with AISI 1080 steel (mesh size 2.5 and 10 mm): (a-b) Specimen 1; (c-d) Specimen 2; (e-f) Specimen 3

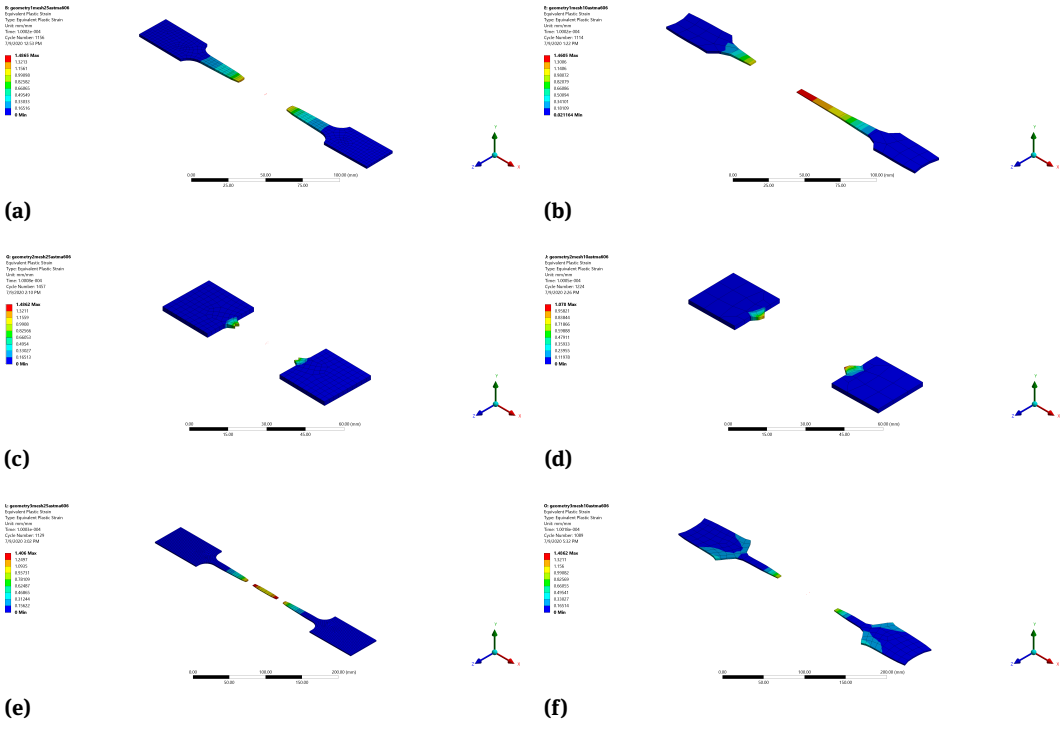

Figure 13: Strain contour of the specimens with HSLA A606 steel (mesh size 2.5 and 10 mm): (a-b) Specimen 1; (c-d) Specimen 2; (e-f) Specimen 3

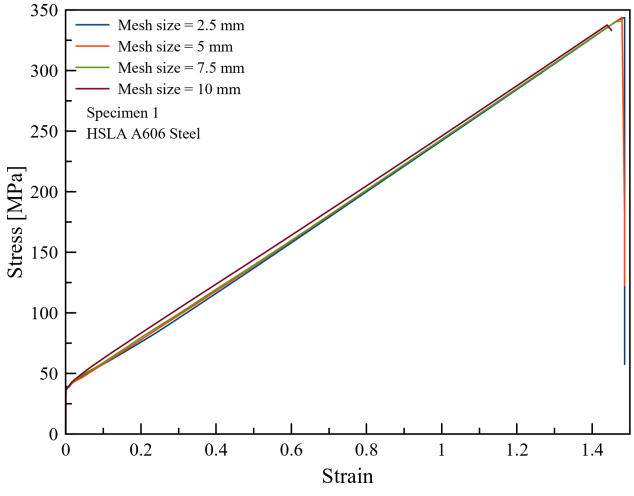

(a)

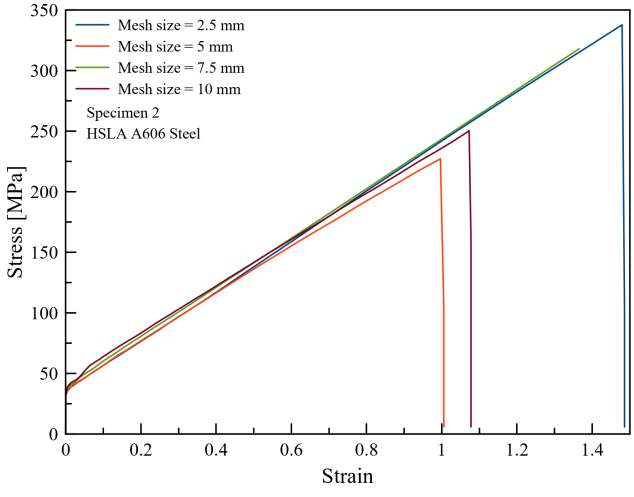

(b)

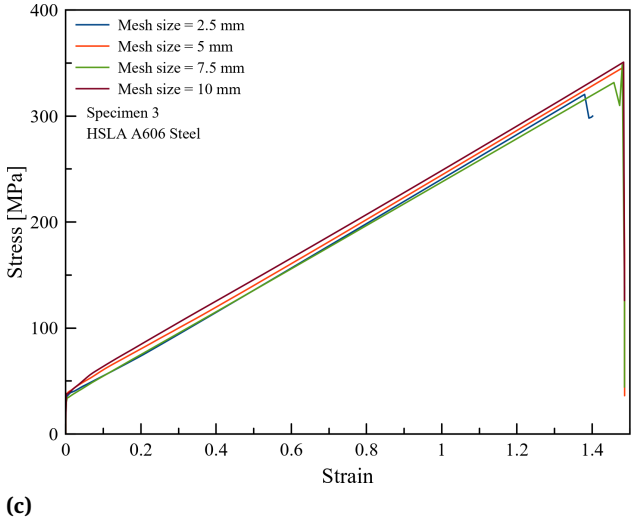

(c)

Figure 14: Geometry characteristics of the specimens with HSLA A606 steel

5.3 Mesh size

Figure 14a, 14c shows that for specimens 1 and 3 with HSLA A606 steel, fractures occurred at a load of around 343.8 MPa and strain of 1.48. For specimen 2, fractures occurred at a load of 337.8 MPa and strain of 1.48 when the mesh size was 2.5 mm. For the same specimen, when the mesh size was 5, 7.5, and 10 mm, fractures occurred at 227.2 MPa, 314.4 MPa, and 250.3 MPa, respectively, as shown in Figure 14b.

5.4 Overall discussion

For the tensile test process, specimens 1 and 3 showed almost the same result in terms of stress and strain values for the three proposed materials. Specimen 2 showed similar results to specimens 1 and 3 when the mesh size was 2.5 mm, but when the mesh size was 5, 7.5, and 10 mm, the stress–strain values were lower for all three proposed materials. In term of von Mises stress, it was found that in specimens 1 and 3 with the three proposed materials, the highest von Mises stress was located in the center of the reduced section of the specimen, and the stress started to expand and reached the grip section. However, for specimen 2, the von Mises stress was found widely distributed over almost the entire specimen in all of the proposed materials. An observation of the strain contour indicated that a significantly different contour was obtained for specimen 2 with a 10 mm mesh size. Besides that finding, the highest strain contour was located in the midsection of all of the specimens in all of the proposed materials.

6 Conclusions

This paper presents a study of the tensile test on different steel materials. A benchmark study was used to ensure that the numerical methodology used in this paper was able to provide reliable results. The geometry of specimens 1 and 3 always showed similar results in all proposed material configurations in terms of stress and strain. The geometry of specimen 2 only showed the same results as specimens 1 and 3 when the mesh size was 2.5 mm. A similar von Mises stress pattern was found in specimens 1 and 3 with all the proposed materials, that is, the highest von Mises stress was located in the center of the reduced section of the specimen, and the stress started to expand and reached the grip section. However, for specimen 2, von Mises stress was found widely distributed over almost the entire specimen in all of the materials. The strain contour results also indicated that there was a significant differ-

ence in the contour obtained when specimen 2 had a 10 mm mesh size. Besides that finding, the biggest strain contour was located in the midsection of all of the specimens with all of the proposed materials.

References

[1] Evans L., Traffic safety, Bloomfield Hills, MI: Science Serving Society, 2004.

[2] Wenzel T.P., Ross M., The effects of vehicle model and driver behavior on risk, Accid. Anal. Prev., 2005, 37(3), 479–494.

[3] Dabadgaonkar S., Sen A.K., Sustainable business model for shipping industry. SFIMAR Research Rev., 2015, 10(1), 19–27.

[4] UNCTAD, Review of Maritime Transport 2017, United Nations Publication, 2017.

[5] Prabowo A.R., Sohn J.M., Bae D.M., Cho J.H., Performance assessment on a variety of double side structure during collision interaction with other ship, Curved Layered Struct., 2017, 4(1), 255–271.

[6] Prabowo A.R., Sohn J.M., Bae D.M., Zakki A.F., Harsritanto B.I.R., Investigating crashworthy single and double skin structures against accidental ship-to-ship interaction, Curved Layered Struct., 2018, 5(1), 180–189.

[7] Prabowo A.R., Muttaqie T., Sohn J.M., Bae D.M., Setiyawan A., On the failure behaviour to striking bow Penetration of impacted marine-steel structures, Curved Layered Struct., 2018, 5(1), 68–79.

[8] Prabowo A.R., Sohn J.M., Putranto T., Crashworthiness performance of stiffened bottom tank structure subjected to impact loading conditions: Ship-rock interaction, Curved Layered Struct., 2019, 6(1), 245–258.

[9] Prabowo A.R., Laksono F.B., Sohn J.M., Investigation of structural performance subjected to impact loading using finite element approach: Case of ship-container collision. Curved Layered Struct., 2020, 7(1), 17–28.

[10] Zhang J., Teixeira A.P., Soares C.G., Yan X., Quantitative assessment of collision risk influence factors in the Tianjin port. Safety Sci., 2018, 110, 363–371.

[11] Chen P., Mou J., van Gelder P.H.A.J.M., Integration of individual encounter information into causation probability modelling of ship collision accidents, Safety Sci., 2019, 120, 636–651.

[12] Vredeveldt A.W. Wevers L.J., Lemmen P.P.M., Full scale ship collision tests, Third International Symposium on Structural Crashworthiness Failure, April 14-16, 1993.

[13] Hu J., Chen W., Fan P., Gao J., Fang G., Cao Z. et al., Uniaxial tensile tests and dynamic mechanical analysis of satin weave reinforced epoxy shape memory polymer composite, Polym. Test., 2017, 64, 235-241.

[14] Yalcin D., How do different specimen geometries affect tensile test results?, ADMET Material Testing, 2017.

[15] Callister W.D., Rethwisch D.G., Materials science and engineering: an introduction, John Wiley & Sons, Inc., 2018.

[16] Törnqvist R., Design of crashworthy ship structures, Technical University of Denmark, 2003.

[17] Chen P., Huang Y., Mou, J., van Gelder P.H.A.J.M., Probabilistic risk analysis for ship-ship collision: State-of-the-art, Safety Sci., 2019, 117, 108–122.

[18] Prabowo A.R., Bae D.M., Sohn J.M., Zakki A.F., Evaluating the parameter influence in the event of a ship collision based on the finite element method approach, Int. J. Tech., 2016, 7(4), 592–602.

[19] Prabowo A.R., Bae D.M., Sohn J.M., Zakki A.F., Cao B., Wang Q., Analysis of structural behavior during collision event accounting for bow and side structure interaction. Theo. App. Mech. Lett., 2017, 7(1), 6–12.

[20] Bae D.M., Prabowo A.R., Cao B., Sohn J.M., Zakki A.F., Wang Q., Numerical simulation for the collision between side structure and level ice in event of side impact scenario, Lat. Am. J. Sol. Struct., 2016, 13(16), 2691–2704.

[21] Prabowo A.R., Sohn J.M., Nonlinear dynamic behaviors of outer shell and upper deck structures subjected to impact loading in maritime environment, Curved Layered Struct., 6(1), 2019, 146–160.

[22] Prabowo A.R., Bahatmaka A., Cho J.H., Sohn J.M., Bae D.M., Samuel S., Cao B., Analysis of structural crashworthiness on a non-ice class tanker during stranding accounting for the sailing routes, Marit. Transportation Harvest. Sea Resour., 2017, 1, 645–654.

[23] Pedersen P.T., Review and application of ship collision and grounding analysis procedures, Mar. Struct., 2010, 23(3), 241–262.

[24] Jose E., Anto T., Analysis of tensile test of mild steel using finite element method, Int. J. Innov. Eng. Tech., 2015, 5(4), 247–251.

[25] Calle M.A.G., Oshiro R.E., Alves M., Ship collision and grounding: Scaled experiments and numerical analysis, Int. J. Impact Eng., 217, 103, 195–210.

[26] Calle M.A.G., Verleysen P., Alves M., Benchmark study of failure criteria for ship collision modeling using purpose-designed tensile specimen geometries, Mar. Struct., 2017, 53, 68–85.

[27] Iannucci L., Rosso S.D, Curtis P.T., Pope D.J., Duke P.W., Understanding the thickness effect on the tensile strength property of Dyneema®HB26 laminates, Mat., 2018, 11(8), 1431.